MTLA 27 (2023) 101682

Contents lists available at ScienceDirect

Materialia

journal homepage: www.elsevier.com/locate/mtla

Influence of processing on the microstructural evolution and multiscale hardness in titanium carbonitrides (TiCN) produced via field assisted sintering technology

Douglas E. Wolfe [a,b,c,d,e,*], Christopher M. DeSalle [a,b], Caillin J. Ryan [a,b], Robert E. Slapikas [a,b], Ryan T. Sweny [a,b], Ryan J. Crealese [a,b], Petr A. Kolonin [a], Sergei P. Stepanoff [a,b], Aman Haque [f], Simon Divilov [g], Hagen Eckert [g], Corey Oses [g], Marco Esters [g], Donald W. Brenner [h], William G. Fahrenholtz [i], Jon-Paul Maria [j], Cormac Toher [g,j], Eva Zurek [k], Stefano Curtarolo [g]

[a] Applied Research Laboratory, The Pennsylvania State University, University Park, PA 16802, United States
[b] Materials Science and Engineering Department, The Pennsylvania State University, University Park, PA 16802, United States
[c] Engineering Science and Mechanics Department, The Pennsylvania State University, University Park, PA 16802, United States
[d] Ken and Mary Alice Lindquist Nuclear Engineering Department, The Pennsylvania State University, University Park, PA 16802, United States
[e] Additive Manufacturing and Design, The Pennsylvania State University, University Park, PA 16802, United States
[f] Department of Mechanical Engineering, The Pennsylvania State University, University Park, PA 16802, United States
[g] Thomas Lord Department of Mechanical Engineering and Materials Science, Center for Autonomous Materials Design, Duke University, Durham, NC 27708, United States
[h] Department of Materials Science & Engineering, North Carolina State University, Raleigh, NC 27695-7907, United States
[i] Department of Materials Science and Engineering Department, Missouri University of Science and Technology, Rolla, MO 65409, United States
[j] Department of Materials Science and Engineering and Department of Chemistry and Biochemistry, University of Texas at Dallas, Richardson, Texas 75080, United States
[k] Department of Chemistry, State University of New York at Buffalo, Buffalo, NY 14260, United States

ARTICLE INFO

Keywords:
Ceramic
FAST
Hardness
Micro-/nanoindentation
Deformation
TiCN

ABSTRACT

Titanium carbonitride (TiCN) is an advanced, high-performance hard ceramic of great commercial importance that has been widely developed and employed. Nonetheless, it has only been in recent years that binderless titanium carbonitride bulk ceramics have been successfully fabricated using field-assisted sintering technology (FAST). However, the underlying structure-processing-property-performance relationships have yet to be fully evaluated, especially concerning indentation hardness of these materials across a broad range of loads and deformation length scales. In this work we aim to address these fundamental relationships and characterize the multiscale hardness phenomena in detail. It was found that the effects of soak temperature and time directly impacted the sintered microstructure and were reflected in the observed mechanical properties over various loads. Valuable insight into the load-dependence of hardness distributions, sensitivity/correlation with elasto-plastic parameters, and multiscale parameterization were developed using micro-/nanoindentation. Particularly, the load-dependent hardness sensitivity and resolvability demonstrate a fundamental tradeoff with respect to the manifested mechanical response influenced by the presence of underlying heterogeneities. These new insights relating the interplay of compositional/microstructural evolution with FAST processing parameters and multi-scale hardness are an important step in advancing next-generation hard ceramics.

1. Introduction

The development of hard ceramics has been crucial to facilitating the universal success of wear-resistant cutting/sliding surfaces in key industrial applications. Historically, the titanium carbonitride system is a distinguished example of a commercial hard ceramic that has been successfully employed for decades due to its superior hardness, tribological properties, thermal stability, corrosion-resistance, and feasible scalability [1–3]. In particular, special attention has been invested in the deposition of these hard materials as coatings onto substrates [4–8].

* Corresponding author at: Applied Research Laboratory, The Pennsylvania State University, University Park, PA 16802, United States.
E-mail address: dew125@arl.psu.edu (D.E. Wolfe).

https://doi.org/10.1016/j.mtla.2023.101682
Received 14 October 2022; Accepted 10 January 2023
Available online 12 January 2023

Although there has been substantial work in describing structure-processing-property-performance relationships of the titanium carbide/nitride-based materials in the form of deposited coatings, significantly less work exists describing these relationships for bulk titanium carbonitride ceramics [9–18].

One of the underlying reasons for this knowledge gap is that conventional sintering of these pure refractory ceramics has been infeasible without the addition of large concentrations of binders/sintering aids that radically degrade the performance of these materials under extreme conditions (esp. hardness) [9]. Nonetheless, implementing novel sintering techniques such as Field Assisted Sintering Technology (FAST) has recently enabled the feasible development of binderless ceramics with superior properties [19–24]. However, even with these substantial advancements in material processing, complete structure-processing-property-performance relationships of hard ceramics with FAST still have not been fully realized. Particularly, the interplay of compositional/microstructural effects on mechanical properties, coupled with the effects of material processing parameters, has not been thoroughly developed. Likewise, special consideration into the multiscale deformation still remains unaddressed and warrants a comprehensive evaluation. As seen in Table A1, the few reported hardness values of bulk titanium carbonitride have been performed under largely disparate loading and processing conditions, making holistic comparisons difficult [25–28]. Therefore, it is critical to investigate these structure-processing-property-performance relationships and multiscale hardness of bulk titanium carbonitride to facilitate measurable improvements in high-performance hard ceramics for applications in extreme environments (i.e. aerospace, hypersonics, manufacturing). This work will address the merits/challenges of multiscale hardness for equitable comparisons and measurable progress in these high-performance hard ceramics. The primary focus of these efforts is to unravel the multiscale hardness phenomena of FAST-processed, binderless titanium carbonitrides for developing new optimization pathways and mechanistic insights for improving these hard ceramics.

2. Experimental

2.1. Powder preparation

Titanium carbide powder (TiC: 4.93 g/cc) with 99.7% purity and quoted average particle size of less than 3 μm was purchased from Inframat Advanced Materials (lot #: IAM7261TIC1). Titanium nitride powder (TiN: 5.22 g/cc) with 99.2% purity and quoted average particle size of 800 nm was purchased from US Research Nanomaterials, Inc. (stock #: US1023M). To reduce the particle size, these powders were independently ball milled using 94% WC-Co 3/16" satellites (Union Process, Inc.). Using 250 ml high-density polyethylene bottles loaded with a 9:1 ball-to-powder mass ratio (BPR) for 80 gs of powder each, subsequent milling at a roller speed of 200 RPM was performed. This was done for 36 h dry, then 68 h wet using anhydrous isopropyl alcohol (60 g) as a dispersant without additional organic additives. The extent of milling on the powders was monitored using laser diffraction (MasterSizer 3000, Malvern Panalytical) with deionized water as the dispersant and 5 min of pre-ultrasonication to reduce agglomeration effects. Afterwards, the milling jars were discharged and the extracted powders were dried in an oven at ~100 °C. These extracted powders were then batched for a 50/50 mol% TiC-TiN mixture, and milled for 10 h (7:1 BPR, 200 RPM) to dry mix these powders.

2.2. FAST processing

The mixed carbide/nitride powders were sintered using a 25 ton FAST system (FCT Systeme GmbH) with 20 mm outer-diameter graphite dies/punches. The internal surfaces of the die body were covered with graphite foil to minimize die degradation and each was loaded with 8 gs of powder. All sintering trials were performed under vacuum (3 mTorr) over a constant heating rate of 100 °C/min and a stepped pressure sequence from 30 to 50 MPa during this heating ramp. In this work, the controlled FAST processing variables were soak temperature (1600–2200 °C) and soak time (5–30 min). As a function of soak temperature series (1600, 1800, 2000, 2200 °C), a constant soak time of 10 min was used, while as a function of soak time trials (5, 15, 20, 30 min), a constant soak temperature of 2000 °C was used. Each sintered sample was subsequently extracted, grit blasted with alumina (100 grit) to remove adherent graphite foil, and the Archimedes densities were measured with a precision digital analytical balance. The relative densities were calculated relative to the stoichiometric TiC/TiN phases and corrected for trace WC media content using the X-ray reference intensity ratio method and helium pycnometry density measurements of pre/post-milled powders (~1-2 wt% WC). These samples were then processed and characterized with scanning electron microscopy (Tescan Mira3 SEM, Bruker Quantax), X-ray diffraction (Empyrean III, Malvern Panalytical XRD), and transmission electron microscopy (FEI Talos F200X TEM) for microstructural and compositional insights.

2.3. Mechanical property testing

For mechanical property characterization, both microindentation and nanoindentation were employed on the relative centers of mounted/polished cross-sections. For Vickers microindentation (Qness Q60 $A+$, ASTM C1327-15), three separate loads (0.5, 1, and 2 kgf) were performed, each with a linear array of 9 indents oriented parallel in the direction of uniaxial pressure and spaced over 5 times the diagonal length (~0.3 mm). For nanoindentation (Bruker Hysitron TI-980, Berkovich tip), two separate loads (2, 3 mN) were performed using 4 × 4 square grids (16 indents) spaced 10 μm apart placed along clear central-equatorial areas. The loading profiles for the indents were quasi-static trapezoids, with 5 s loading/unloading times and 2 s hold times, where the hardness was measured using the Oliver-Pharr method. Between sessions, appropriate fused quartz calibrations and tip cleanings were routinely performed. After collection, all measured hardness values and force-displacement loading/unloading curves were plotted and screened for defects and outliers (i.e. curve discontinuities or abnormal profiles), before further analysis.

3. Results and discussion

3.1. Materials processing

We have observed significant size class reduction under these milling conditions for the TiC and TiN powders as shown in Fig. 1a and 1b. For example, the 10–50th percentile particle sizes (Dv10–50) showed a 44–68% reduction, which yielded colloidal particles spanning 0.3–1 μm respectively. The presence of the colloidal primary particles was confirmed by SEM analysis, as shown in Fig. 1c and d. The post-milling particle morphology appeared moderately angular but with relatively equiaxed particles spanning over comparable size ranges between TiC and TiN. This commensuration of distinct powder particle size distributions into more similar size classes allows for higher packing densities and maximum interfacial particle contact area for improved sintering and homogenization. Furthermore, due to the Hall-Petch relationship, smaller particle sizes is necessary for obtaining finer, harder microstructures [29]. Therefore, these ball milling efforts have demonstrated effective comminution and commensuration of TiC/TiN powder for subsequent FAST processing to achieve dense, fine-grained microstructures.

After the powder processing, subsequent FAST processing of the 50/50 TiC-TiN mixtures across various soak temperatures and times was performed and the Archimedes densities measured (see Table 1).

For the soak temperature series, temperatures at or above 1800 °C lead to apparent saturation in relative density (~96%). Similar trends were also observed for soak times at or above 15 min, but with a slight

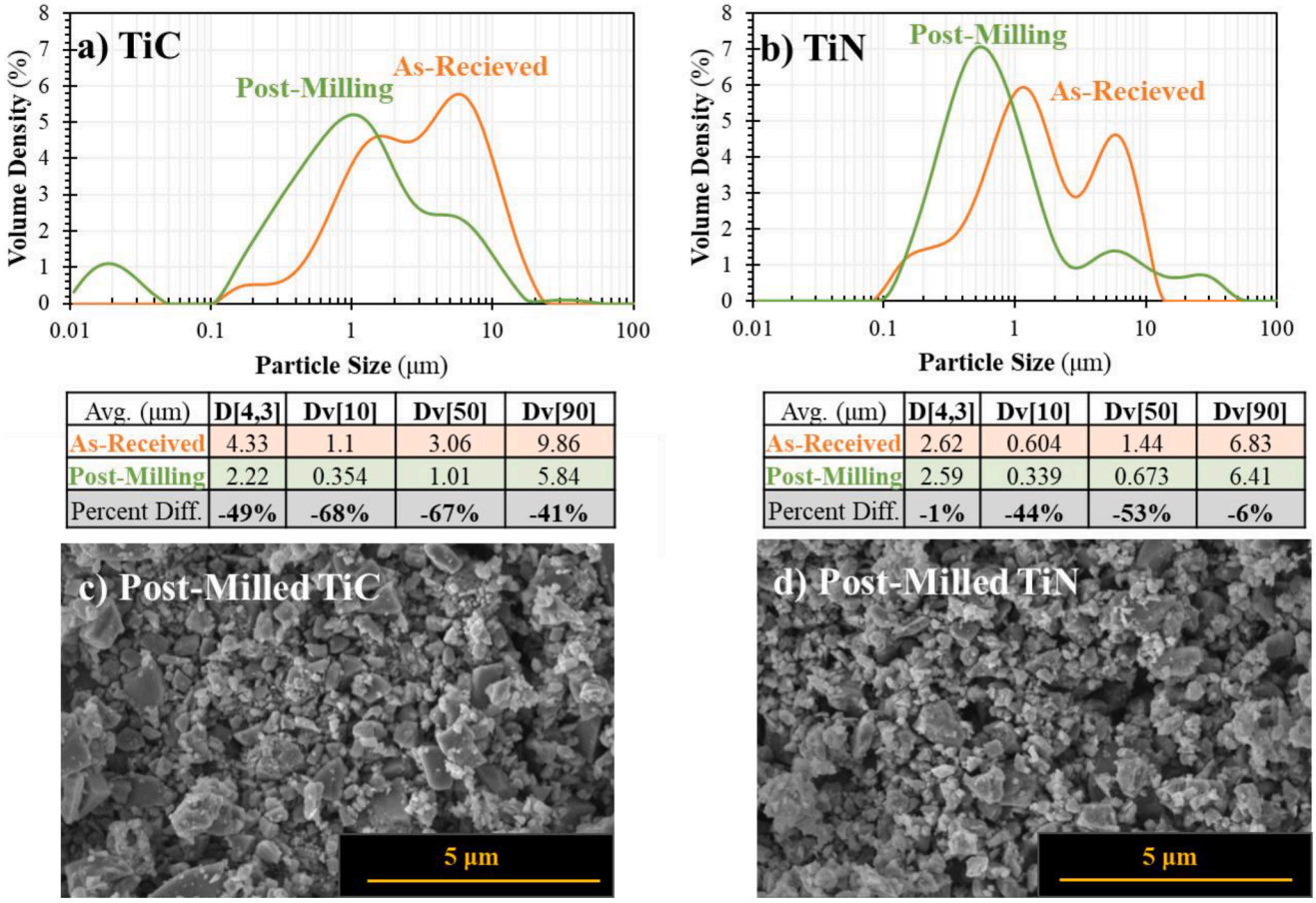

Avg. (μm)	D[4,3]	Dv[10]	Dv[50]	Dv[90]
As-Received	4.33	1.1	3.06	9.86
Post-Milling	2.22	0.354	1.01	5.84
Percent Diff.	-49%	-68%	-67%	-41%

Avg. (μm)	D[4,3]	Dv[10]	Dv[50]	Dv[90]
As-Received	2.62	0.604	1.44	6.83
Post-Milling	2.59	0.339	0.673	6.41
Percent Diff.	-1%	-44%	-53%	-6%

Fig. 1. (a) TiC particle size distributions and (b) TiN particle size distributions measured with laser diffraction. (c) Post-milled TiC and (d) post-milled TiN particles resolved with SEM.

Table 1
Tabulated FAST sintering soak conditions for 50/50 TiC-TiN ceramics with respective Archimedes relative densities.

Series	Temperature (°C)	Time (min)	Relative Density (%)	*Error (%)
Temperature	1600	10	94.7	0.64
	1800	10	96.2	0.36
	2000	10	96.4	0.24
	2200	10	96.2	0.27
Time	2000	5	96.1	0.17
	2000	15	96.6	0.31
	2000	20	96.6	0.44
	2000	30	96.8	0.35

* Propagation of error from measurement error and relative variability.

monotonic increase. This suggests that the FAST soak temperatures (≥ 1800 °C) have sufficient thermally-activated densifying diffusion mechanisms to complete intermediate-stage sintering and transition into final-stage sintering. However, the kinetics of the final-stage sintering process is substantially slower than the intermediate-stage and therefore require significantly longer soak times for incremental densification improvements. These incremental gains in densification during final stage sintering are typically mediated by grain growth, leading to an underlying tradeoff in hardness between density and coarsening effects. Hence, it is first necessary to examine the effects of these fundamental soak parameters (i.e. temperature, time) for establishing viable generalizations before tuning other processing parameters such as applied pressure or additives.

3.2. Structural characterization

To characterize the crystalline phases present, XRD analysis in Fig. 2 of these sintered TiC/TiN ceramics was performed across all FAST sintering conditions. The peak positions confirm that all the ceramics are primarily composed of the expected single-phase carbonitrides, since all the measured average lattice parameters fell within ± 0.01 Å of the expected $TiC_{0.5}N_{0.5}$ value. However, we observe that moving from 1600 to 2200 °C for a constant soak time of 10 min results in a significant reduction in peak width (~150–330% FWHM decrease). This may be attributed to homogenization, as the underlying peaks of the TiC/TiN parent phases convolute to a greater extent when the microstructure is less homogenized, appearing effectively as a broader peak. A similar trend is observed for the 5–30 min soak time series held at 2000 °C, but the peaks were comparatively less pronounced (~10–70% FWHM decrease). To conclusively attribute the extent of the phase homogenization, microstructures to these soak temperature and time series using SEM analysis were resolved and compared in Fig. 3. This figure supports the homogenization description observed in XRD, as the 2200 °C-sintered microstructure appears vastly more uniform than the heterogeneous 1600 °C-sintered microstructure. The Z-contrast in the backscattering electron images indicates spatial variation in composition, which appears as shades of gray where lighter regions generally indicate nitrogen-rich and darker carbon-rich.

The compositional variations were resolved using EDS in Fig. 4 and used to classify key microstructural features. The bright white speckles in Fig. 4a and f appeared tungsten-rich and are attributed as trace WC content from the milling media. The dark elongated regions surrounded with carbon in Fig. 4b and d appear as phases of segregated carbon.

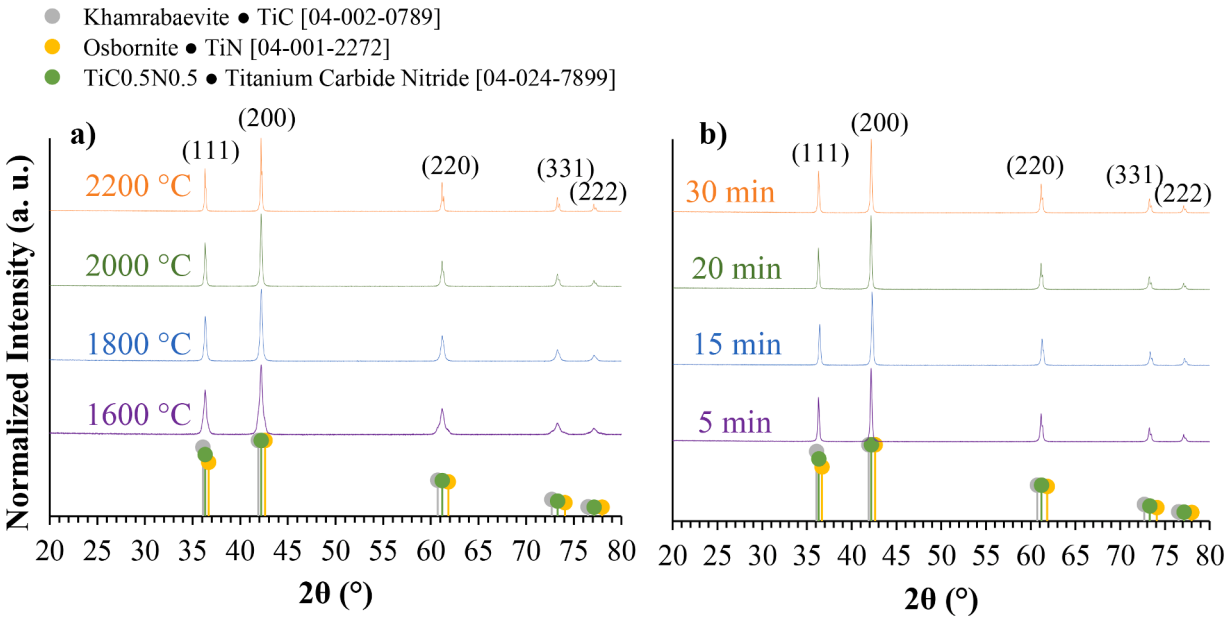

Fig. 2. XRD overlay comparison of (a) FAST sintering soak temperature effects at 10 min soaks, (b) FAST soak time effects at 2000 °C soaks for 50/50 TiC-TiN ceramics.

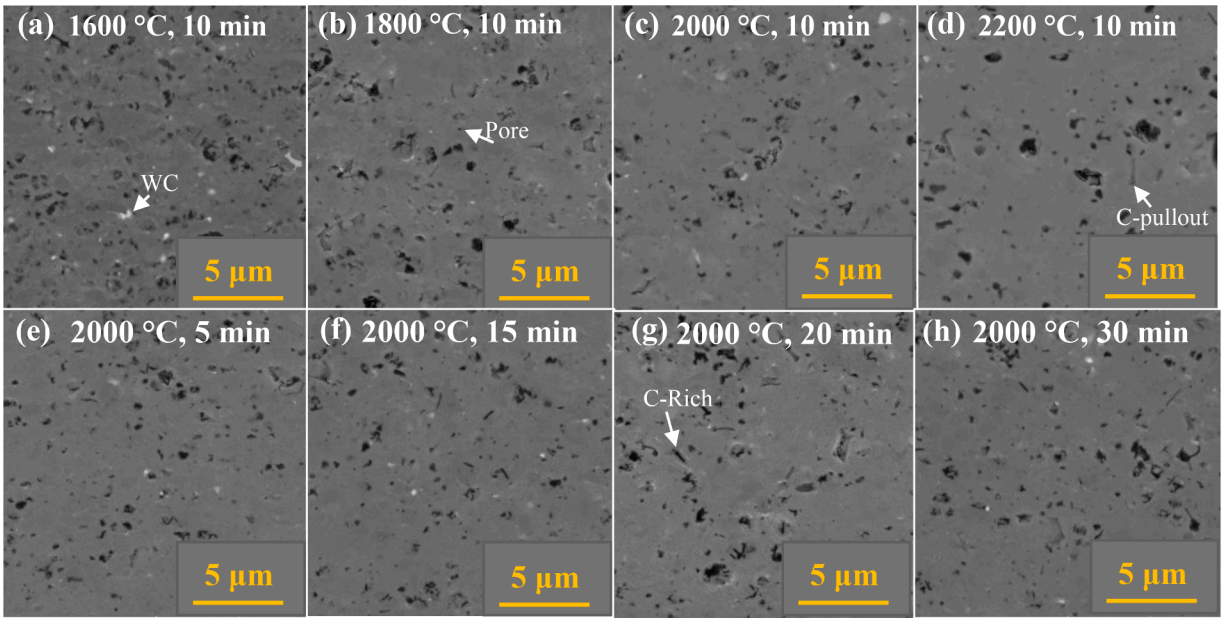

Fig. 3. SEM micrographs of polished cross-section FAST 50/50 TiC-TiN ceramics for soak conditions of (a) 1600 °C/10 min, (b) 1800 °C/10 min, (c) 2000 °C/10 min, (d) 2200 °C/10 min, (e) 2000 °C/5 min, (f) 2000 °C/15 min, (g) 2000 °C/20 min, and (h) 2000 °C/30 min, respectively.

Likewise, dark spherical regions appear to be intrinsic pores while more sharp/angular dark features are attributed to "pull-out" grinding defects. These pull-out defects are a result of the large hardness contrast between the soft carbon-rich secondary phases and the hard titanium carbonitride primary matrix phase, where the carbon tends to be preferentially removed from the microstructure during processing and artificially contributes to the observed porosity. The intrinsic pores however tend to lie along grain boundaries and are generally difficult to differentiate from pull-out/carbon-rich phases. Nonetheless, applying higher current/voltage electron beam settings selectively charges pores to reveal them in contrast to the conductive carbon/$TiC_{0.5}N_{0.5}$ microstructure and other techniques such as dark field optical microscopy also provides further differentiation of these pores. To obtain greater insights into these complex microstructures, more advanced quantitative micrographic analysis methods (e.g. electron backscatter diffraction mapping) that can correlate the compositional attributes of SEM-EDS with resolved microscopic structures are needed to fully quantify the phase fraction and respective size distribution of the microstructural features. Qualitatively however it is still clear that the heterogeneity observably decreases with higher soak temperatures due to greater homogenization of the mixed TiC/TiN green body into the single-phase $TiC_{0.5}N_{0.5}$ alloy with more thermally-activated diffusion.

Based on these respective homogenization insights, further TEM analysis was performed on the most homogenous 2200 °C/10 min $TiC_{0.5}N_{0.5}$ ceramic to characterize the atomic-level nanostructure. As seen in Fig. 5a, the principal phases observed are the $TiC_{0.5}N_{0.5}$ and

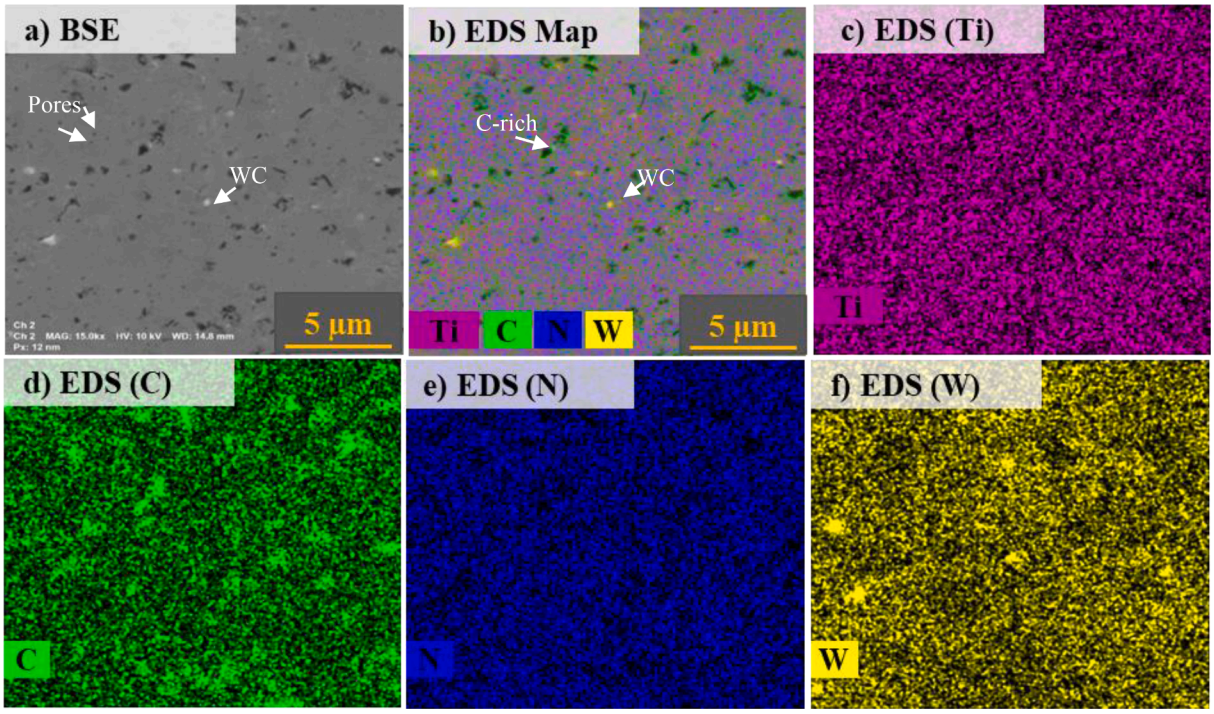

Fig. 4. SEM-EDS elemental mapping of FAST 50/50 TiC-TiN (2000 °C/15 min) with (a) BSE micrograph, (b) EDS map, (c) Ti content (pink), (d) C content (green), (e) N content (blue), and (f) W content (yellow).

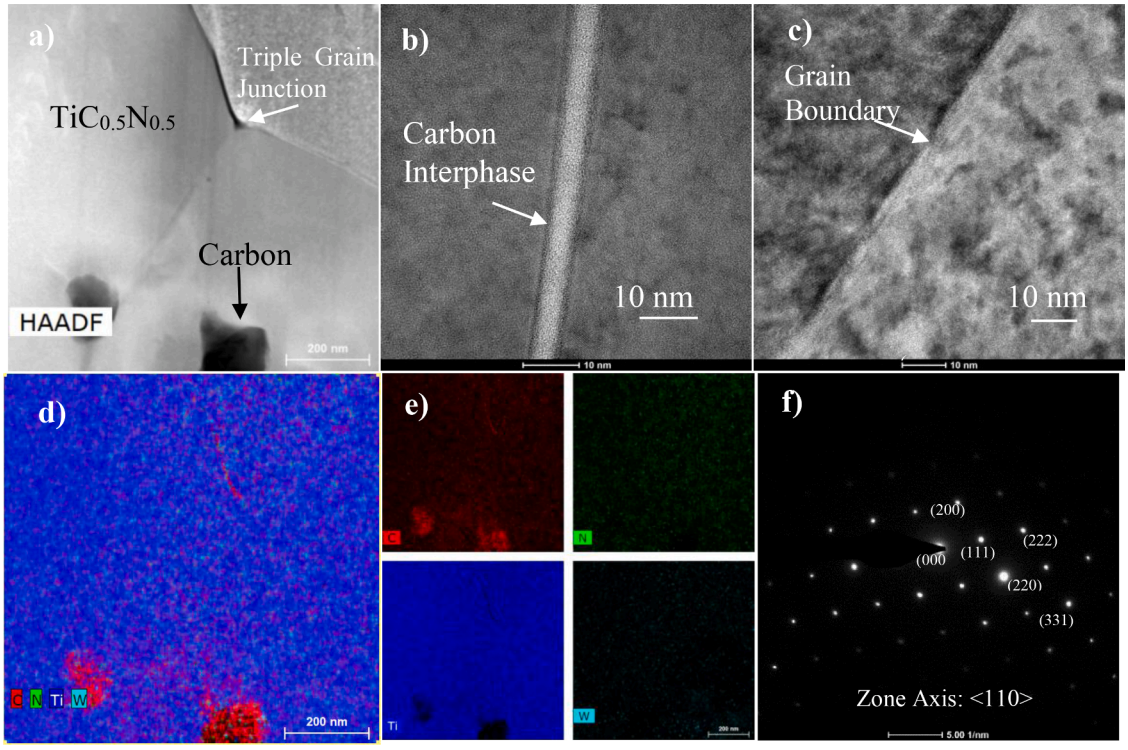

Fig. 5. TEM micrographs of $TiC_{0.5}N_{0.5}$ interfaces (2200 °C/10 min soak), (a) Triple grain junction, (b) Segregated carbon-rich interphases, (c) Carbon-free grain boundary, (d) EDS of triple grain junction, (e) EDS individual element maps, and (f) SAED electron diffraction pattern of $TiC_{0.5}N_{0.5}$ phase.

carbon. The carbon phases appear most prominently in the EDS maps of Fig. 5d and e, while the Selected Area Electron Diffraction (SAED) pattern in Fig. 5f confirmed the same predominant $TiC_{0.5}N_{0.5}$ cubic phase resolved in XRD. In Fig. 5b, several nanometer-wide interphases of carbon along a grain boundary are evident, suggesting the structure has no clear long-range order (i.e. amorphous). We find that clear grain boundaries, such as in Fig. 5c, appear more carbon-free between these carbonitride grains as well.

The appearance of the isolated carbon phases in SEM and TEM suggests the existence of a significant driving force for segregating

carbon/nitrogen atoms at these elevated soak temperatures. Even though these $TiC_{0.5}N_{0.5}$ FAST-processed ceramics should behave as ideal single-phase solid solutions, in reality, there are pre-existing chemo-mechanical gradients and interfacial segregation developed under even the most homogenizing of processing conditions. Despite other contributing factors such as precursor stoichiometry and free carbon impurities which can influence this, the favorability of these segregated carbon phases at these elevated temperatures for 50/50 C:N molar ratios is supported by relevant thermodynamic assessments, but models have not yet been validated for predicting Ti-C-N phase stability under the non-equilibrium, field-assisted conditions of FAST [30]. Moreover, determining the effect of these soft carbon phases in a $TiC_{0.5}N_{0.5}$ ceramic matrix on the overall apparent hardness is crucial for optimizing the processing of the binderless carbonitride FAST ceramics.

3.3. Mechanical characterization

In Fig. 6, SEM micrographs comparing the significant size differences of microindents and nanoindents on the TiC/TiN FAST ceramic microstructures is shown. Fig. 6a and b illustrate clearly how microindentation nominally probes microscale intergranular-microstructural effects, while nanoindentation in Fig. 6c shows more localized sensitivity to nanoscale intragranular-compositional effects with respect to hardness. With microindentation, contributions from primary/secondary phases across many deformed grains and local porosity leads to the apparent hardness response to be more representative of the overall microstructure. In the case on nanoindentation however, since the imprint size (~200–500 nm) is generally smaller than the grain size of the constituent phases, the deformation response is more localized and the probed hardness is representative of the phase itself, without Hall-Petch or porosity effects being superimposed. We measured the load-dependence of the sampled hardness distributions from the function of soak temperature and time series with these pooled data sets. The distribution comparisons presented in Fig. 7a and b demonstrate a notable transition from normal, symmetric hardness distributions at high microindentation loads (~15–18 GPa microhardness) to more skewed, non-normal apparent hardness distributions at low nanoindentation loads (~10–33 GPa nanohardness). These values are comparable to the average hardness range in Table A.1 (~21–33 GPa) for these titanium carbonitrides and their constituent endmembers (TiC: 28–35 GPa, TiN: 18–21 GPa), but the underlying hardness distributions of these materials have not been previously compared [31].

The changes in apparent hardness distribution are critical considerations when comparing differences in hardness between material systems at various loads. In reality, it is infeasible to determine the full functional form of the true hardness distribution for each sample, as hundreds to thousands of indents per sample would be required per load. With these considerations, a systematic methodology is needed to reasonably account for this distributed hardness effect when directly drawing relative comparisons. To quantify these hardness distributions, nonparametric and parametric quantities have been employed respectively. Nonparametrically, a median bounded by the 90th and 10th percentile bounds best represents the majority of the measured hardness, as this middle 80% is robust to the upper/lower 10% of potential extreme or outlier values. Parametrically, an average bounded with a confidence interval (i.e. 95%+) best represents the center of mass or central moment to the data, enabling facile signal detection.

As seen in Fig. 8, this type of analysis has been applied to compare hardness differences across the set of 50/50 TiC-TiN ceramics fabricated with various soak conditions. In the case of microhardness in Fig. 8c, as the applied load decreases, the apparent hardness at higher soak temperatures (2000–2200 °C) slightly increases. This may be attributed to both the slight reduction in porosity and the higher degree of homogenization present which results in solid solution strengthening, where lower loads would have greater sampling sensitivity from microstructural defects (i.e. pores, heterogeneities) as the probed length scale decreases. In Fig. 8d, the effect of soak time with decreasing applied load, however, appears to be invariant to load and only uniformly shifts microhardness to higher values. This suggests the differences in the phase fractions of these associated defects across soak time is minimal, which was previously corroborated with SEM in Fig. 4b. This is further reinforced by the strikingly similar nanohardness values (medians ~25–28 GPa) between different soak times seen in Fig. 8b, as the apparent hardness being sampled on the local nanoscale did not notably vary across soak time due to less significant solid solution strengthening or phase evolution occurring over these time scales. Meanwhile, the changes in nanohardness as a function of soak temperatures in Fig. 8a are comparatively more pronounced, where the lower 2 mN applied load is more distinct than the higher 3 mN load nanohardness. This further substantiates the correlated microstructural differences with these defect densities seen in microhardness for varying soak temperatures. In particular, it appears that the pronounced peak in sampled hardness with the 2 mN load suggests significant physiochemical changes occurring at these smaller length scales. Most likely this can be attributed to the three competing phenomena that are operant. At the low temperature regime of 1600 °C, consolidation is dominant from the active sintering kinetics, but yields a more nanocomposite-like structure that tiles the milled TiC/TiN powder grains together. This type of structure has the greatest heterogeneity and the least solid solution strengthening, leading to a softer and wider hardness distribution. From 1800 to 2000 °C, sufficient thermally-activated diffusion occurs to homogenize these local compositional gradients and introduce solid solution strengthening of the titanium carbonitride matrix grains, creating a more diffuse/homogenous composite structure with harder and

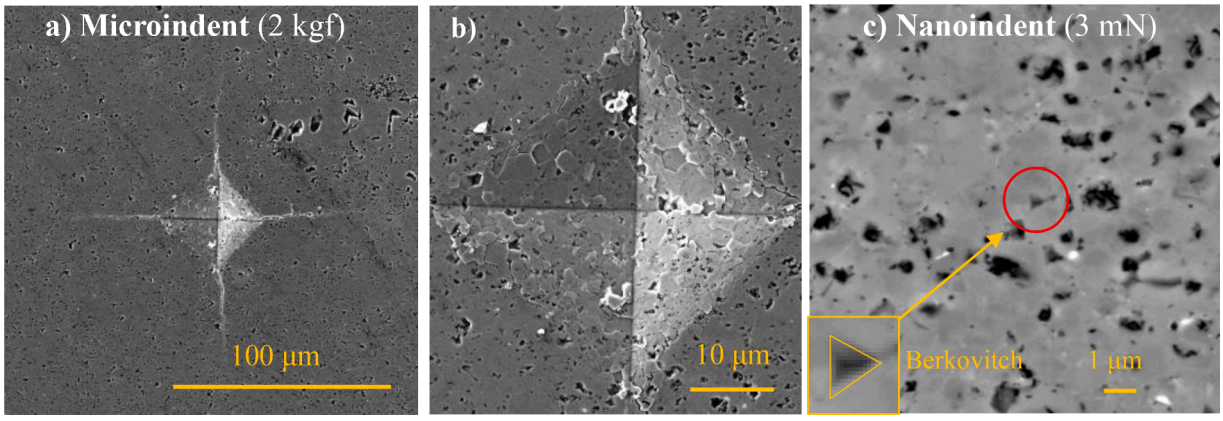

Fig. 6. SEM micrograph examples of (a) Vickers microindent at 2 kgf, (b) Close-up of microindentation, and (c) Berkovitch nanoindent at 2 mN, for relative size comparison on TiC/TiN FAST-processed ceramic microstructure.

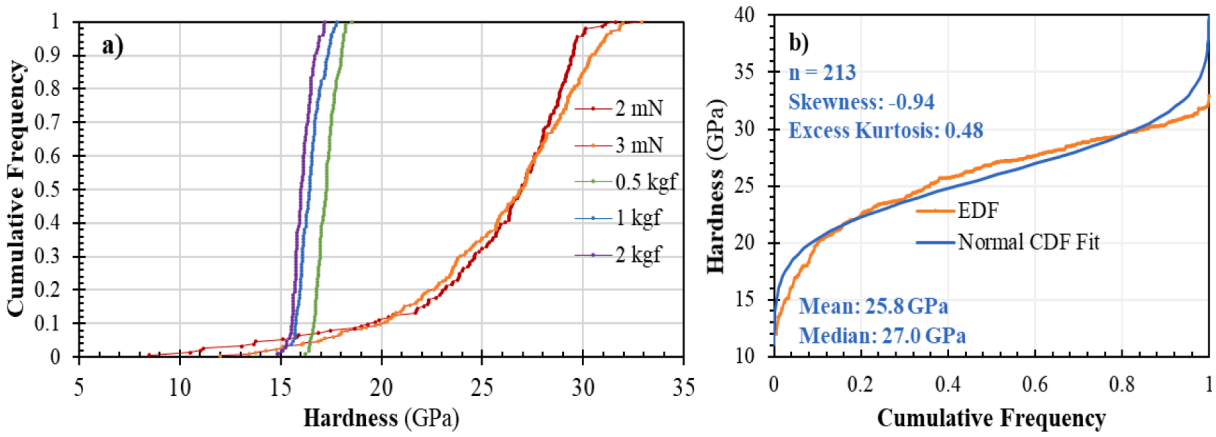

Fig. 7. (a) Apparent load-dependence of observed pooled hardness distributions (b) Pooled nanohardness distribution normality fit comparison at 3 mN load.

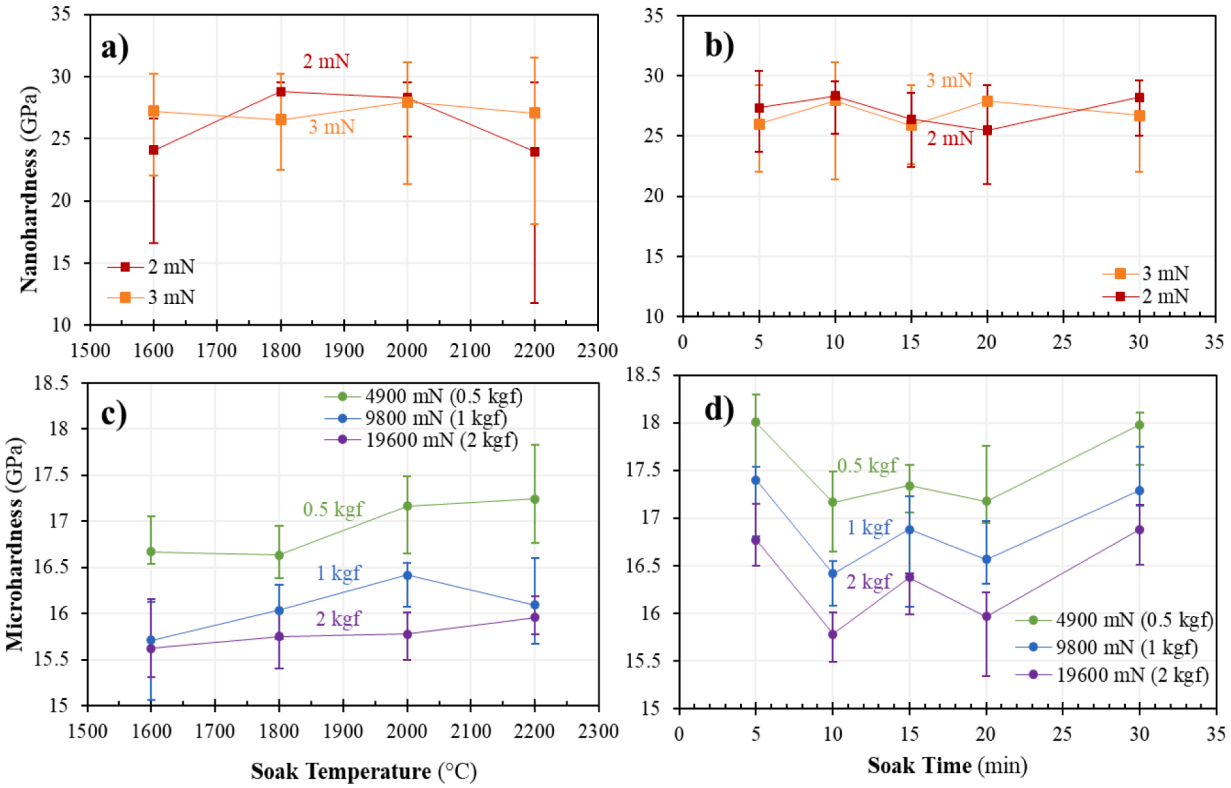

Fig. 8. (a) Nanohardness comparisons across various soak temperatures and (b) soak times. (c) Microhardness comparisons across various soak temperatures and (d) soak times (plotted points are medians bounded with 90th/10th percentile error bars).

narrower hardness distributions. At the highest soak temperature of 2200 °C, the intergranular segregation and growth of the softer carbon-rich secondary phases begins to dominate and the localized carbon depletion of the primary titanium carbonitride phase leads to reduced hardness because less carbon content generally leads to lower hardness in carbonitride systems. The greater variability in the hardness distribution for 2200 °C soak temperature results from probing this more microcomposite-like structure of C-deficient titanium carbonitride primary phases mixed with larger C-rich phases. Therefore, the measured nanohardness reflects this microstructural evolution across soak temperatures as a result of the competing effects of consolidation, solid solution strengthening, and carbon segregation. Although the apparent hardness sensitivity is enhanced when probing at lower loads, the clear tradeoff to balance is the increased variability and skewness associated with these microstructural defects. Hence, using multiple loads is necessary to resolve apparent hardness differences in these ceramics.

Consequently, to further explore these fundamental differences between each of these processing conditions, the parametric approach was taken in comparing the most sensitive differences at the lowest loads with nanoindentation across the other relevant elastoplastic parameters. As seen in Fig. 9a, correlated changes between the max indentation depth and the nanohardness are more pronounced at the lower 2 mN applied load for the function of temperature series, but they also correlate in Fig. 9b to the function of time series as well. Since shallower indents tend to yield smaller contact areas, this correlation substantiates the relative nanohardness differences observed. Furthermore, these differences in apparent hardness are reinforced by the independent elastoplastic measurements that were derived from the respective loading/unloading curves.

These measurements include the reduced modulus, which represents

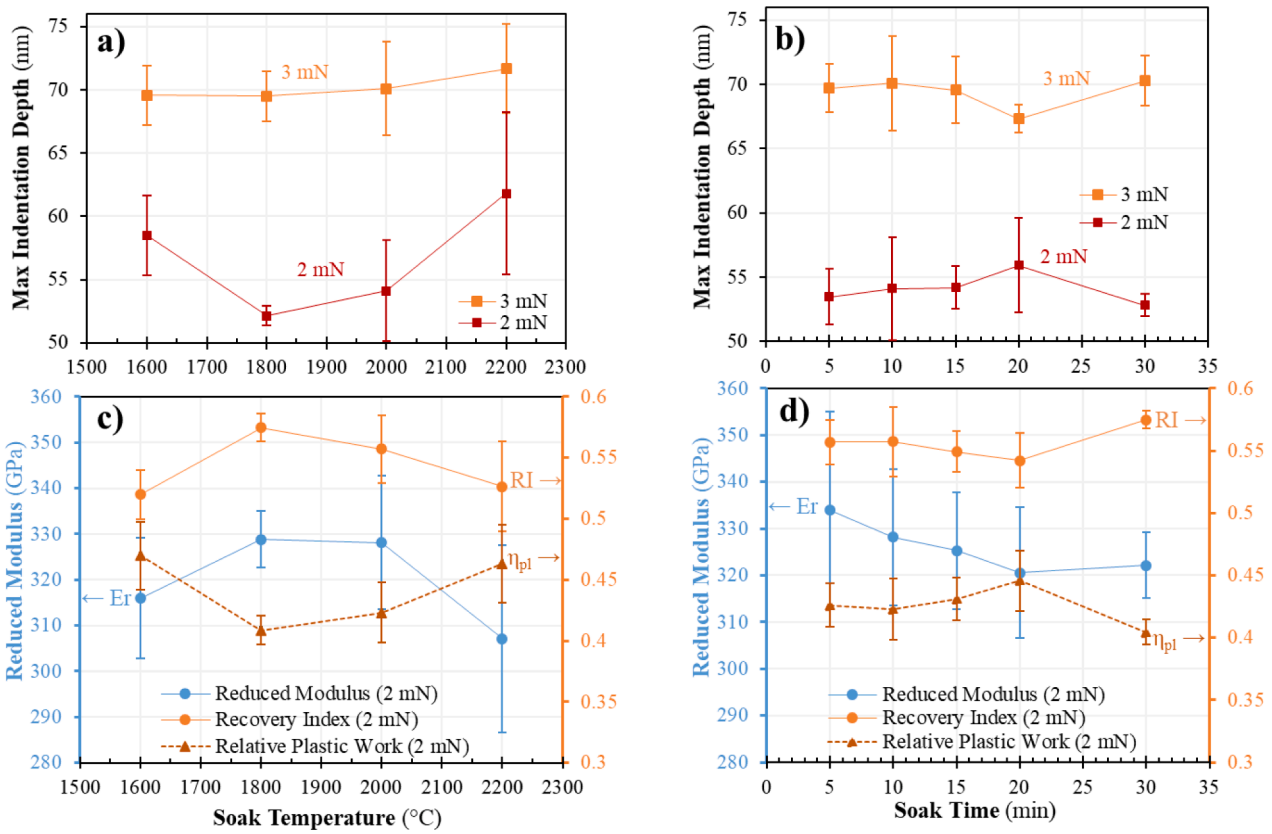

Fig. 9. (a) Nanohardness max indentation depths comparison for soak temperature and (b) soak time. (c) Correlated nanoindentation elastoplastic measurements comparison at 2 mN load for soak temperature and (d) soak time for FAST $TiC_{0.5}N_{0.5}$ ceramics (average bounded with 95% confidence interval).

the resistance to elastic deformation of the sample relative to the diamond tip. Likewise, the elastic recovery index, which quantifies the extent of elasticity using the relative recoverable depth during unloading. Lastly, the relative plastic work, which denotes the fraction of plastic work dissipated during indentation, quantifies the extent of plasticity on an energy basis. Collectively these elastoplastic parameters fully characterize the mechanical response of the material during indentation and are necessary to holistically evaluate relative hardness changes.

For instance, in Fig. 9c and d, the recovery index positively correlates with the measured 2 mN nanohardness and is negatively correlated with the max indentation depth. This corroborates that harder materials at low loads tend to demonstrate more elastic behavior, as the high resistance to plastic deformation compels more observable elastic deformation to accommodate the applied mechanical load. Additionally, the negative correlation between the relative plastic work and recovery index supports this, as lower plasticity implies higher elasticity in these elastoplastic materials. Lastly, the reduced modulus appears to be correlated with the recovery index. Assuming the hardness remained constant, a greater resistance to elastic deformation would promote more favorable plastic deformation to occur, which should lead to higher observed plasticity. Instead, the greater resistance to elastic deformation is coupled with increased elasticity, which strongly suggests the resistance to plastic deformation increased accordingly. The overall curved peak shape of the profile and point variability for these elastoplastic quantities in Fig. 9c correlates and support the nanohardness observations described in Fig. 8a with respect to soak temperature microstructural effects. Likewise in Fig. 9d, a flatter curve is observed and correlates with the nanohardness profile of Fig. 8b, but to a lesser extent due to the minimal effect of soak time on FAST-induced microstructural transformations relative to soak temperature.

Nonetheless, to unify the microhardness and nanohardness results into a multiscale hardness description of these materials, the load dependence must be correspondingly accounted for. The appropriate model most commonly used to describe this load-dependence is an empirical power law fit. In Fig. 10, the fitting parameters derived from the average respective hardness values at each load is summarized. As previously determined with the independent microhardness and nanohardness analysis, the greatest resolvable differences observed are due to the effect of soak temperatures on homogenization and phase fraction of hardness-sensitive heterogeneities.

These resolvable soak temperature differences are reflected in Fig. 10a, while the soak time series demonstrates comparatively smaller differences as seen in Fig. 10b. For soak temperature series, the general profile of these power law fit trends appear to mostly track with that of the 2 mN nanohardness measurements, suggesting the evolution of nanoscale heterogeneities is most influential in predicting the full load-dependence of hardness. Meanwhile, the fit parameters for the soak time series more closely resemble the profile of the microhardness measurements, suggesting the minimal differences in nanoscale heterogeneities do not strongly influence the overall hardness response and is instead more microstructurally-sensitive. These extracted multiscale hardness results manifest the physiochemical observations characterized by XRD, SEM, and TEM, directly establishing structure-processing-property-performance relationships between FAST soak conditions and the mechanical properties demonstrated from respective $TiC_{0.5}N_{0.5}$-based ceramics. Moreover, this approach facilitates mechanistic insights into unraveling the many contributions to hardness at various length scales to enable optimized materials processing and compositional design improvements. In the case of the titanium carbonitride system, the optimal soak conditions were 1800–2000 °C held for 10 min due to the interplay of competing consolidation, solid solution strengthening, and carbon-segregation effects at various temperature regimes. To augment the hardness and overall wear-resistant performance of these ceramics,

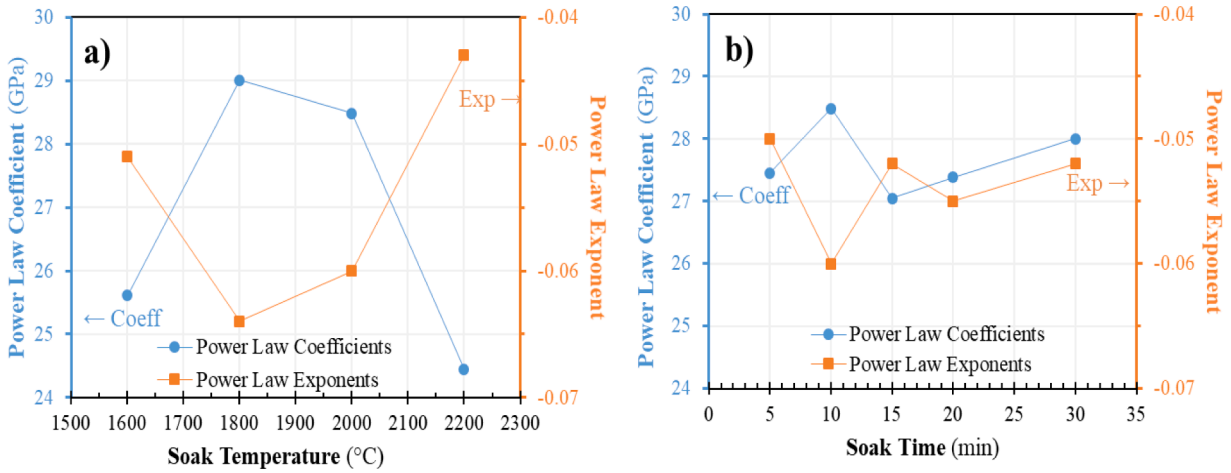

Fig. 10. (a) Multiscale average power law fits as a function of soak temperature and (b) soak time for FAST $TiC_{0.5}N_{0.5}$ ceramics from 2 mN to 2 kgf loads.

maximizing hardness enhancements (i.e. Hall-Petch effect, solid solution strengthening), and minimizing detrimental softening effects (i.e. carbon depletion, weaker secondary phases, porosity) are fundamentally necessary to push the boundaries of modern hard ceramics. Therefore, by combining nanohardness and microhardness insights into unified multiscale hardness, more judicious treatments of load-dependence can be further realized to enable improved hardness comparisons between these materials for the advancement of next-generation hard ceramics.

4. Conclusion

1. Binderless titanium carbonitride ceramic alloys were successfully fabricated with effective independent ball milling and FAST processing parameters to realize dense, fine-grained ceramics with varying levels of microstructural complexity based on different soak conditions.
2. Structural characterization techniques such as XRD, SEM, and TEM determined microstructural and nanostructural physiochemical differences across various FAST soak conditions. These differences were attributed to the effect of soak temperature and time on the degree of phase homogenization and fraction of residual heterogeneities. Specifically, competitive mechanisms such as consolidation, solid solution strengthening, and carbon segregation were attributed as the most influential to the apparent hardness at various soak temperature regimes. At the lower soak temperatures of 1600 °C, the consolidation of a more nanocomposite-like TiC/TiN structure is developed, while a more microcomposite-like C-depleted Ti(C,N)/C-rich structure is developed from carbon segregation at the higher soak temperature of 2200 °C. At intermediate soak temperatures, solid solution strengthening effects are maximized with formation of homogenous Ti(C,N) alloys with minimal carbon segregation. Meanwhile soak time exhibited minimal differences in measured hardness because of its lower effect on the extent of diffusion observed in FAST processing relative to temperature.
3. Independent nanohardness and microhardness results demonstrated differences in the apparent hardness distributions and the tradeoff between hardness sensitivity/resolvability with respect to the influence these heterogeneities have on the overall mechanical response of $TiC_{0.5}N_{0.5}$ ceramics. A higher load and larger indent area (i.e. microindentation) results in greater microstructural averaging of constituent phases and defects in the measured hardness. Meanwhile, lower load or smaller indent areas (i.e. nanoindentation) collectively yield more diverse ranges of resolved hardness that are unique to the individual probed phases.
4. Nanohardness differences across these FAST soak conditions were substantiated by the self-consistent correlated changes in the measured elastoplastic properties and provide a more holistic description of the underlying mechanical response in these materials. These elastoplastic properties provided additional further insights into the changes in the intrinsic mechanical resistances and the extents of deformation.
5. Multiscale hardness differences as a function of soak temperature and time illustrate the significant influence compositional/microstructural heterogeneities possess across various length scales. For the case of titanium carbonitrides, soak temperatures of 1800–2000 °C held 10 min provided an optimal hardness regime due to sufficient diffusion to provide solid solution strengthening with minimal excess carbon segregation. It is the development of these structure-processing-property-performance relationships that will advance the development of harder FAST-processed ceramics for high-performance, wear-resistant applications under extreme conditions. In particular, this work provides the groundwork for opportunities to further enhance hardness of ceramics and to unravel contributions to multiscale hardness in order to facilitate greater strength and wear-resistance across various application-relevant loading conditions.

Ownership/originality statement

We declare that this submitted work is our own and copyright has not been breached in seeking this publication. Additionally, this original work has not been published in full or being considered for publication elsewhere.

Declaration of Competing Interest

The authors declare that they have no known competing financial interests or personal relationships that could have appeared to influence the work reported in this paper.

Acknowledgments

We would like to gratefully acknowledge the DoD SPICES MURI sponsored by the Office of Naval Research (Naval Research contract N00014-21-1-2515) for their financial support of this work.

Supplementary materials

Supplementary material associated with this article can be found, in the online version, at doi:10.1016/j.mtla.2023.101682.

References

[1] J. He, F. Zhang, P. Mi, Y. Qin, K. Chen, Y. Yang, et al., Microstructure and wear behavior of nano C-rich TiCN coatings fabricated by reactive plasma spraying with Ti-graphite powders, Surf. Coat. Technol. 305 (2016) 215–222. Nov.

[2] P.K. Ajikumar, M. Kamruddin, S. Kalavathi, A.K. Balamurugan, S. Kataria, P. Shankar, et al., Synthesis, characterization and evaluation of titanium carbonitride surface layers with varying concentrations of carbon and nitrogen, Ceram. Int. 38 (3) (2012) 2253–2259. Apr.

[3] W. Feng, H. Zhou, Y.S. Ze, Nano-indentation and wear-resistance behaviors of TiCN films by pulsed plasma on cemented carbide cutting tool, Mater. Sci. Eng. A 527 (18–19) (2010) 4767–4770. Jul.

[4] L. Qiu, Y. Du, S. Wang, L. Du, Z. Chen, J. Wang, et al., Through-process modeling and experimental verification of titanium carbonitride coating prepared by moderate temperature chemical vapor deposition, Surf. Coat. Technol. 359 (2019) 278–288. Feb.

[5] K. Balázsi, I.E. Lukács, S. Gurbán, M. Menyhárd, L. Bacáková, M. Vandrovcová, et al., Structural, mechanical and biological comparison of TiC and TiCN nanocomposites films, J. Eur. Ceram. Soc. 33 (12) (2013) 2217–2221. Oct.

[6] L. Chen, S.Q. Wang, Y. Du, J. Li, Microstructure and mechanical properties of gradient Ti(C, N) and TiN/Ti(C, N) multilayer PVD coatings, Mater. Sci. Eng. A 478 (1–2) (2008) 336–339. Apr.

[7] P.C. Siow, J.A. Ghani, M.J. Ghazali, T.R. Jaafar, M.A. Selamat, H.C.H. Che, Characterization of TiCN and TiCN/ZrN coatings for cutting tool application, Ceram. Int. 39 (2) (2013) 1293–1298. Mar.

[8] Y. Qin, H. Zhao, C. Li, J. Lu, J. He, Effect of heat treatment on the microstructure and corrosion behaviors of reactive plasma sprayed TiCN coatings, Surf. Coat. Technol. 398 (2020), 126086. Sep.

[9] D. Wolfe Sythnesis and characterization of TiC, TiBCN, TiB2/TiC and TiC/CrC multilayer coatings by reactive and ion beam assisted, electron beam-physical vapor deposition (EB-PVD) [Doctoral Thesis]. The Pennsylvania State University; 2001.

[10] S. Kumar, D.E. Wolfe, M.A. Haque, Dislocation shielding and flaw tolerance in titanium nitride, Int. J. Plast. 27 (5) (2011) 739–747. May.

[11] E. Alat, M.J. Brova, I.M. Younker, A.T. Motta, M. Fratoni, D.E. Wolfe, Neutronic and mechanical evaluation of rare earth doped and undoped nitride-based coatings for accident tolerant fuels, J. Nucl. Mater. 518 (2019) 419–430. May.

[12] E. Alat, A.T. Motta, R.J. Comstock, J.M. Partezana, D.E. Wolfe, Multilayer (TiN, TiAlN) ceramic coatings for nuclear fuel cladding, J. Nucl. Mater. 478 (2016) 236–244. Sep.

[13] D.E. Wolfe, J. Singh, Titanium carbide coatings deposited by reactive ion beam-assisted, electron beam–physical vapor deposition, Surf. Coat. Technol. 124 (2–3) (2000) 142–153. Feb.

[14] D.E. Wolfe, J. Singh, K. Narasimhan, Synthesis and characterization of multilayered TiCyTiB$_2$ coatings deposited by ion beam assisted, electron beam–physical vapor deposition, Surf. Coat. Technol. 18 (2003).

[15] D.E. Wolfe, J. Singh Microstructural evolution of titanium nitride (TiN) coatings produced by reactive ion beam-assisted, electron beam physical vapor deposition (RIBA, EB-PVD). [Master's Thesis]. The Pennsylvania State University; 1996.

[16] B. Borawski, J.A. Todd, J. Singh, D.E. Wolfe, The influence of ductile interlayer material on the particle erosion resistance of multilayered TiN based coatings, Wear 271 (11–12) (2011) 2890–2898. Sep.

[17] D. Wolfe, A. Motta, E. Timothy. Ceramic coating for corrosion resistance of nuclear fuel cladding US20180294062A1, 2018. p. 19. Available from: https://patents.google.com/patent/US20180294062A1/en?inventor=Douglas+E.+Wolfe&oq=Douglas+E.+Wolfe.

[18] J. Wang, Y. Liu, J. Ye, S. Ma, J. Pang, The fabrication of multi-core structure cermets based on (Ti,W,Ta)CN and TiCN solid-solution powders, Int. J. Refract. Met. Hard Mater. 64 (2017) 294–300. Apr.

[19] O.J. Akinribide, B.A. Obadele, S.O. Akinwamide, H. Bilal, O.O. Ajibola, O. O. Ayeleru, et al., Sintering of binderless TiN and TiCN-based cermet for toughness applications: processing techniques and mechanical properties: a review, Ceram. Int. 45 (17) (2019) 21077–21090. Dec.

[20] P. Angerer, L.G. Yu, K.A. Khor, G. Korb, I. Zalite, Spark-plasma-sintering (SPS) of nanostructured titanium carbonitride powders, J. Eur. Ceram. Soc. 25 (11) (2005) 1919–1927. Jul.

[21] Y. Li, H. Katsui, T. Goto, Preparation of ZrCN−TiCN solid solutions by spark plasma sintering, Ceram. Int. 43 (18) (2017) 16965–16971. Dec.

[22] I. Zalite, P. Angerer, L.G. Yu, K.A. Khor, Spark-plasma-sintering (SPS) of tungsten carbide and titanium carbonitride nanopowders, IOP Conf. Ser. Mater. Sci. Eng. (2011), 012039. Jun23;23.

[23] D.E. Wolfe, P.E. Albert, C.J. Ryan, J.A. Reiss, S.P. Stepanoff, P.A. Kolonin, Optimized processing of high density ternary hafnium-tantalum carbides via field assisted sintering technology for transition into hypersonic applications, J. Eur. Ceram. Soc. 42 (2) (2022) 327–335. Feb.

[24] P. Sarker, T. Harrington, C. Toher, C. Oses, M. Samiee, J.P. Maria, et al., High-entropy high-hardness metal carbides discovered by entropy descriptors, Nat. Commun. 9 (1) (2018) 4980. Dec.

[25] G.N. Mekgwe, O.J. Akinribide, T. Langa, B.A. Obadele, P.A. Olubambi, L. M. Lethabane, Effect of graphite addition on the tribological properties of pure titanium carbonitride prepared by spark plasma sintering, IOP Conf. Ser. Mater. Sci. Eng. 3 (499) (2019), 012011. Apr.

[26] B.M. Moshtaghioun, J.M.M. Chávez, F.L. Cumbrera, D.G. García, Titanium carbonitride fabricated by spark plasma sintering: is it a ceramic model of carbon-induced Friedel-Fleisher strengthening effect? J. Eur. Ceram. Soc. 41 (13) (2021) 6275–6280. Oct.

[27] O. Zgalat-Lozynskyy, M. Herrmann, A. Ragulya, Spark plasma sintering of TiCN nanopowders in non-linear heating and loading regimes, J. Eur. Ceram. Soc. 31 (5) (2011) 809–813. May.

[28] G.N. Mekgwe, O.J. Akinribide, S.O. Akinwamide, P.A. Olubambi, Fabrication of graphite reinforced TiCxNy by spark plasma sintering technique: a comparative assessment of microstructural integrity and nanoindentation properties, Vacuum 187 (2021), 110144. May.

[29] H. Ryou, J.W. Drazin, K.J. Wahl, S.B. Qadri, E.P. Gorzkowski, B.N. Feigelson, et al., Below the Hall–Petch limit in nanocrystalline ceramics, ACS Nano 12 (4) (2018) 3083–3094. Apr 24.

[30] S. Jonsson, Calculation of the Ti-C-N system, Int. J. Mater. Res. 87 (9) (1996) 713–720. Sep 1.

[31] H.O. Pierson, Handbook of Refractory Carbides and Nitrides: Properties, Characteristics, Processing, and Applications, Noyes Publications, Park Ridge, N.J, 1996, p. 340.